Structural characterization of amorphous alumina and its polymorphs from first-principles XPS and NMR calculations

Raquel Lizárraga,[1] Erik Holmström,[1] Stephen C. Parker,[2] and Corinne Arrouvel[3]
[1]*Instituto de Física, Facultad de Ciencias, Universidad Austral de Chile, Casilla 567, Valdivia, Chile*
[2]*Department of Chemistry, University of Bath, Bath BA2 7AY, United Kingdom*
[3]*Universidade Federal de Sergipe, Depto de Física, São Cristóvão, Sergipe 49.100-000, Brazil*
(Received 19 October 2010; published 14 March 2011)

We have calculated x-ray photoemission (XPS) spectra and nuclear magnetic resonance (NMR) chemical shifts for amorphous alumina from first principles. We generate models for amorphous structures at three different densities by means of a stochastic quenching procedure. We analyze these structures by calculating radial distribution functions, angle distributions functions, bond lengths, and coordination numbers. Our amorphous models compare well with previous molecular dynamics simulations and experiments. We include in our study, the stable phase of alumina α, some of the transition phases, that is, θ, γ, and κ, and the hypothetical bixbyite structure for comparison. Our results reproduce both XPS spectra and NMR chemical shifts and suggest that the XPS failure to resolve the different local environments in the different phases of alumina is due to the strong ionicity of the Al-O bond. Our calculated NMR chemical shifts show that the local environments are well resolved. We estimate the broadening of the NMR peaks due to local atomic environment differences in the amorphous phase to be as large as 35 ppm.

DOI: 10.1103/PhysRevB.83.094201 PACS number(s): 61.43.−j, 81.05.Rm

I. INTRODUCTION

Structural determination can be very challenging, especially for disordered materials such as amorphous systems. The lack of order in these systems makes the interpretation of experiments that are commonly used to analyze the structure of crystalline materials difficult. Aluminum oxide, Al_2O_3, also known as alumina, is an example of such a complex system.

Alumina is a technologically important ceramic material. Its resistance and insulating properties have led to its widespread use in electronic devices as a corrosion-resistant film.[1] It is also employed in catalysis, for example, hydrodesulfuration[2,3] and in Na-S batteries.[4] There exist several transition alumina phases. The thermodynamically stable phase is the so-called α-Al_2O_3 whose crystal structure is well known.[5–7] However, the crystal structure of some of the transition phases are not well established. Alumina can also be stabilized in an amorphous state. The interest in this phase has increased considerably because the amorphous phase is linked to many important applications such as a high-k dielectric,[8] in catalysis,[9] luminescence,[10] and optical devices,[11] and as a precursor in the process of manufacturing well-defined crystalline materials.[12]

Despite the vast number of studies[5,6,13–15] on alumina, many uncertainties remain and many contradicting results have been reported. For example, even though nuclear magnetic resonance (NMR) is an experimental technique suited to perform local environment analysis, different ratios of coordination numbers for amorphous alumina (a-Al_2O_3) have been found.[15–17] X-ray photoemission (XPS) is also a powerful experimental method that provides information on the local environment and chemical compositions. However, XPS experiments appear to fail in distinguishing different atomic environments for the different alumina phases and therefore provide little insight in the issue.[18,19] Furthermore, the density of the amorphous phase of alumina varies over an exceptionally large range, between 2.1 and 3.5 g/cm^3 (Refs. 20–22) which raises the question of the existence of amorphous polymorphism.[23] This phenomenon has been observed before in Al_2O_3-Y_2O_3.[24] On the theory side, molecular dynamics (MD) simulations have been carried out on a-Al_2O_3, yielding contradictory results on coordination numbers.[25,26] Therefore, the characterization of the a-Al_2O_3 phase remains an unsolved problem.

Density functional theory (DFT)[27,28]-based methods have proved to be highly accurate in predicting properties of crystalline alumina phases[29,30] as well as XPS spectra of amorphous phases of other metal oxides.[31,32] They have also shown to be very successful at aiding the interpretation of NMR experiments in microporous Al compounds.[33] This shows that experimental techniques and DFT calculations can complement each other to produce a very accurate description of materials.

In this paper, we investigate the structural properties of models of the a-Al_2O_3 phase, at three different densities, $\rho = 2.9$, 3.1, and 3.3 g/cm^3, by means of first-principles DFT calculations and compare them to the crystalline phases α, θ, γ, and κ. In our study we have also included the bixbyite alumina phase that, although it has not been observed, it may be used to establish trends due to its highly ordered structure. We compute the XPS and NMR spectra from first principles for a-Al_2O_3 and some of the crystalline alumina phases. We construct the models for a-Al_2O_3 by using a stochastic quenching method that has been shown to be successful in describing the properties of amorphous structures.[34–36] We verify the validity of our models for a-Al_2O_3 by calculating radial distribution functions, angle distribution functions, bond lengths, and coordination numbers

and we compare our results to previous MD simulations and experiments.

II. THEORY

A. Stochastic quenching procedure

In order to calculate the XPS and NMR spectra from first principles the positions of the atoms in the amorphous structure need to be known. The structural models for a-Al_2O_3 used in this study were obtained by employing a simple and very efficient quenching method that has recently been used to probe the underlying potential landscape of Na[34] and to calculate accurately the equilibrium density and bulk modulus of a metallic glass system.[35] The procedure can be described as follows: We start by constructing an initial configuration of 200 atoms (80 aluminum and 120 oxygen atoms) that are distributed randomly in a cubic box with a constraint that limits the closeness of approach of any pair (0.4 Å). The volume of the cell was taken according to the density of the amorphous structure. In this study we performed calculations for densities 2.9, 3.1, and 3.3 g/cm^3. The positions of the atoms in the initial configurations were then relaxed using a first-principles DFT method; the Vienna *ab initio* simulation package (VASP).[37,38]

B. First-principles XPS spectra

In an XPS experiment, the photoelectron binding energy is measured as

$$E_B = \hbar\omega - E_{\rm kin} + E_{\rm ref}, \tag{1}$$

where $\hbar\omega$ is the x-ray photon energy, $E_{\rm kin}$ is the kinetic energy of the photoelectron measured with a detector, and $E_{\rm ref}$ is a reference that depends on the Fermi levels of the sample and the detector.

XPS spectra can be calculated from first principles for a wide range of systems including bulk metals,[43] surface structures,[44] metallic interfaces,[45] and amorphous oxides.[31] In order to obtain an XPS spectrum we first compute the site-dependent binding-energy differences. For Al_2O_3 the binding-energy differences can be expressed as

$$\Delta E_B = E(Al_{2-x}Al^*_xO_3) - E(Al_2O_3), \tag{2}$$

where $E(Al_{2-x}Al^*_xO_3)$ is the total energy of the supercell with a concentration of core-ionized atoms x equal to one over the number of Al atoms in the supercell. In the pseudopotential method we are using in this study we cannot directly ionize a core electron. A way around this problem is to approximate the excited atom, Al*, by adding a proton to the nucleus, that is, the next element of the periodic table.[46] This approach is called the $Z+1$ approximation and it has been shown to produce very good results on amorphous CdTeO oxides.[31,32] We have also tested the $Z+1/2$ approximation[47] that is based in the Slater-Janak transition rule[48] applied to DFT. As seen before in other studies,[47] both approximations yield similar results. For the sake of clarity, in Fig. 3 we present only the CLS obtained by using the $Z+1$ approximation.

In order to obtain an XPS spectrum a Gaussian function of standard deviation 0.1 eV was associated with each site-dependent binding-energy difference.[49] Finally, the Gaussians are all summed up to form the continuous line of the XPS spectrum.

C. First-principles NMR chemical shift

When a uniform magnetic field $\mathbf{B}$ is applied to a sample, it induces an electrical current. The strength of the external fields that are typically used in NMR experiments generates electronic currents, $\mathbf{j}^{(1)}(\mathbf{r}')$ that are proportional to the external field $\mathbf{B}$. In turn, the first-order induced current $\mathbf{j}^{(1)}(\mathbf{r}')$ produces a nonuniform magnetic field,[50,51]

$$\mathbf{B}^{(1)}_{\rm int}(\mathbf{r}) = \frac{1}{c}\int d^3r'\,\mathbf{j}^{(1)}(\mathbf{r}')\times\frac{\mathbf{r}-\mathbf{r}'}{|\mathbf{r}-\mathbf{r}'|^3}. \tag{3}$$

The first-principles calculation ultimately yields the absolute chemical shielding tensor, $\overleftrightarrow{\sigma}$, defined as[52]

$$\mathbf{B}^{(1)}_{\rm int}(\mathbf{r}) = -\overleftrightarrow{\sigma}(\mathbf{r})\mathbf{B}. \tag{4}$$

To calculate the chemical shielding tensor, first $\mathbf{j}^{(1)}(\mathbf{r}')$ is obtained by perturbation theory and then $\mathbf{B}^{(1)}_{\rm int}(\mathbf{r})$ is evaluated from the expression in Eq. (3).

The isotropic chemical shielding is given by $\sigma_{\rm iso}(\mathbf{r}) = {\rm Tr}[\overleftrightarrow{\sigma}(\mathbf{r})]/3$. In an NMR experiment the isotropic chemical shift $\delta_{\rm iso}$ is measured and it is related to the isotropic shielding by

$$\delta_{\rm iso} = -(\sigma_{\rm iso} - \sigma_{\rm ref}). \tag{5}$$

The external reference $\sigma_{\rm ref}$ can be chosen differently, usually an $Al(H_2O)_6{}^{3+}$ or $AlCl_3$ solution. In our calculations the isotropic chemical shifts were referenced to α-Al_2O_3, that is, 532.27 ppm for ^{27}Al.

The electric field gradient (EFG) tensor can also be computed. If the eigenvalues of the EFG tensor are labeled V_{xx}, V_{yy}, and V_{zz} so that $|V_{zz}| \geqslant |V_{yy}| \geqslant |V_{xx}|$, then the quadrupolar coupling constant, that is, the coupling between the nuclear electric quadrupole moment eQ and the EFG, is defined as[53]

$$C_Q = \frac{eQV_{zz}}{h} \tag{6}$$

and the asymmetry parameter η is defined as

$$\eta = \frac{V_{xx} - V_{yy}}{V_{zz}}, \tag{7}$$

where e is the absolute value of the electron charge and h is the Planck constant.

The sign of C_Q cannot be determined at room temperature from a simple NMR magic angle spinning (MAS) spectrum, and so absolute values of C_Q are considered experimentally. The calculated values for C_Q are, however, exact and therefore we report negative values as well in Table III.

In our calculations an experimentally determined quadrupole moment, eQ, of 146.6 mB was used for ^{27}Al.[54] The calculated NMR spectra are produced in a similar manner as the calculated XPS spectra with a standard deviation of 3 ppm of the Gaussian broadening functions. This procedure results in a spectrum where the peak areas are perfectly proportional to the Al coordination numbers. Caution must then be taken when comparing the calculations to measurements since this is not the case in experiments.[15]

III. COMPUTATIONAL DETAILS

Total energy calculations were performed within DFT implemented in VASP[37,38] together with the Perdew, Busrke, and Ernzerhof (PBE) parametrization[55] of the exchange-correlation functional. The eigenstates of the electron wave functions were expanded on a plane-waves basis set using pseudopotentials to describe the electron-ion interactions within the projector augmented waves approach.[56] The convergence criterion for the electronic self-consistent cycle was fixed at 10^{-7} eV/cell and the forces on all ions were smaller than 10^{-5} eV/Å. We used a cutoff energy of 300 eV for the polycrystalline and the amorphous phases. A convergence on the k-point meshes using Monkhorst-Pack[57] was ensured. Structural optimizations were performed by using a standard conjugate gradient method during the stochastic quenching procedure.

NMR chemical shifts were calculated using CASTEP.[58] This is a DFT-based code that utilizes the gauge including projected augmented wave (GIPAW) algorithm to handle the reconstruction of the all-electron wave function in a magnetic field. Since the amorphous structures were optimized with VASP, a single point calculation was done with the CASTEP PBE functional. On-the-fly pseudopotentials were used to describe the core-valence interactions. In order to reproduce the same accuracy of the VASP calculations with CASTEP, a higher energy cutoff of 850 eV on the kinetic energy was employed. For ^{27}Al, the $3s$ and $3p$ states were considered in the valence with a core radius of 2.0 Å.

IV. RESULTS AND DISCUSSIONS

A. Structural analysis

1. Al_2O_3 crystalline polymorphs

In this section, we present some structural properties of α-alumina, the transition alumina phases θ, γ, κ, and the hypothetical bixbyite phase. The experimental and calculated densities and lattice constants for each alumina phase are listed in Table I. The calculated shortest O-O, Al-Al, and Al-O bonds, average Al-O bond, and coordination numbers are also displayed in Table I. Aluminum coordination numbers are denoted by Al_{IV} (fourfold), Al_V (fivefold), and Al_{VI} (sixfold). We have employed a structure for the hypothetical bixbyite alumina that corresponds to the cubic bixbyite Mn_2O_3.[59] We find excellent agreement between our calculated and available experimental lattice constants and bond lengths of α, θ, and κ alumina phases.

X-ray diffraction (XRD) experiments are traditionally used to obtain accurate structures of crystalline materials. However, for amorphous systems, the diffraction pattern ultimately only provides the radial distribution function which represents an average over the entire structure. The details of the local atomic structures can therefore not be resolved. The problem may occur as well in complex crystalline structures such as γ-alumina where the structure is believed to be based on a spinel structure with defects.[60] The positions of the defects have not yet been well determined and therefore the structure of γ-alumina is still a topic of discussion in the literature.[61,62] Moreover, it is known that γ-alumina is not a well-defined crystal since its structure depends on the degree of crystallinity of this phase and the transformation process to produce it, which complicates the matter further.[42,63,64]

In this work we have chosen a model for γ-alumina derived by Krokidis *et al.* (see Refs. 42 and 65) that is not a defective spinel. This model has been shown to reproduce XRD patterns,[42,66] temperature-programmed desorption (TPD), and infrared (IR) spectra.[30,67,68] The percentage of Al_{IV} was estimated by means of NMR spectroscopy[69] to be between 25% and 30%, which is consistent with the value for our model of γ-alumina and MD simulations based on structural parameters from Ref. 70. Krokidis *et al.* developed their model from the dehydration of the γ-boehmite structure with a tetragonal distortion, namely, γ_T-alumina. A cubic form, γ_C-alumina, has also been observed by other routes of synthesization, that is, thermal oxidation of the a-Al_2O_3 and chemical vapor deposition. Nevertheless, the most commonly reported structure for γ-Al_2O_3 is the cubic spinel-like structure (space group $Fd3$-mz).[60] In Table I, the experimental values for γ-Al_2O_3 were taken from the work of Krokidis *et al.*

TABLE I. Experimental and calculated structural properties of α-alumina, the transition alumina phases θ, γ, κ, and the hypothetical bixbyite structure. The calculated total energies for each phase with respect to the α-Al_2O_3 phase are listed as well.

	α		κ		Bixbyite	θ		γ	
Polymorph	Expt.[5,39]	Theory	Expt.[40]	Theory	Theory	Expt.[41]	Theory	Expt.[42]	Theory
Density (g/cm^3)	3.98	3.88	3.77	3.68	3.75	3.61	3.53	3.60	3.61
a (Å)	4.76	4.80	4.83	4.87	8.97	11.80	11.89	7.94	7.9
b (Å)	4.76	4.80	8.31	8.38	8.97	2.91	2.94	7.94	7.93
c (Å)	12.99	13.11	8.94	9.00	8.97	5.62	5.66	7.86	8.07
Shortest O-O (Å)	2.52	2.55	2.55	2.55	2.49	2.44	2.56	2.66	2.53
Shortest Al-Al (Å)	2.65	2.68	2.79	2.86	2.95	2.91	2.93	1.71	2.67
Shortest Al-O (Å)	1.85	1.87	1.70	1.75	1.87	1.70	1.77	1.70	1.75
Average Al-O (Å)	1.91	1.93	1.91	1.91	1.93	1.87	1.87	1.86	1.90
Al_{IV} (%)	0		25		0	50		25	
Al_V (%)	0		0		0	0		0	
Al_{VI} (%)	100		75		100	50		75	
Energy per Al_2O_3 (eV)	0		0.11		0.11	0.06		0.16	

TABLE II. Calculated structural properties of a-Al_2O_3 at three densities 2.9, 3.1, and 3.3 g/cm^3 compared to experimental values and an MD study.

Density (g/cm^3)	2.9	3.1	3.3	3.3 (MD Ref. 25)	Expt.
Average O-O (Å)	2.75	2.72	2.81	2.75	2.8 ± 0.58[14]
Average Al-Al (Å)	3.20	3.15	3.13	3.12	3.2 ± 0.55[14]
Average Al-O (Å)	1.85	1.84	1.85	1.76	1.8 ± 0.21[14]
Average Al coordination	4.44	4.52	4.78	4.38	4.1[14], 4.64[13], 4.81[13]
Al_{III} (%)	6.25	7.5	0	0	0[15], 20[14]
Al_{IV} (%)	47.5	37.5	30	65	55 ± 3[15], 56[14]
Al_V (%)	42.5	50.0	61.25	31	42 ± 3[15], 22[14]
Al_{VI} (%)	3.75	5	8.75	4	3 ± 2[15], 0[14]

κ-Al_2O_3 is another alumina phase that has not been yet well characterized. In this work we used a model from Ref. 71 that yields good values of lattice parameters and bond lengths.

The most stable phase of alumina is α in which all Al ions are sixfold coordinated. The trend observed in the polymorphs of alumina is that the number of Al_{VI} decreases toward lower densities while the crystal structure becomes less stable. This is supported by thermodynamic measurements[72] that predict the following order of stability: $\gamma < \kappa < \alpha$. The θ phase was not observed in that study. Similar energy differences to the ones in Table I have been found by other studies.[73,74]

We point out here that the fact that γ-Al_2O_3 appears to not comply with the trend observed in the other polymorphs can be understood as a consequence of an ambiguity in the γ structure. A close inspection of the γ structure reveals that one Al_{VI} ion has one long Al-O bond (2.02 Å) with an oxygen atom that simultaneously belongs to a Al_{IV} environment with a much shorter bond (1.80 Å). The Al_{VI} environments that contain long Al-O bonds may hence be interpreted as intermediate configurations between sixfold and fivefold coordination. In the calculated NMR spectra (Fig. 4) for γ-Al_2O_3 we observe that the peak assigned to Al_{VI} is split into a pure Al_{VI} peak and an intermediate peak between the peaks assigned to Al_{IV} and Al_{VI} that contain these intermediate Al_{VI} configurations.

2. *Amorphous Al_2O_3*

We have characterized our amorphous structures by means of the radial distribution function (RDF), angle distribution function (ADF), number of nearest neighbors, and Al-O distances.

In Table II we summarize some calculated structural properties of a-Al_2O_3 and compare them with a previous MD study[25] and experiments.[13–15] Bond lengths and coordination numbers have been obtained by using cutoffs from RDFs in Fig. 1. Our average O-O, Al-Al, and Al-O bond lengths of the amorphous models are in excellent agreement with both experiments and MD calculations. The average Al coordination number is higher in our calculations than the MD results for the same density. We notice that our value of the average coordination number corresponding to $\rho = 3.1$ g/cm^3 agrees well with the experiments of Ref. 13 which were performed at a similar density $\rho = 3.05$ g/cm^3.[75] However, experiments[13–15] find that the average Al coordination number ranges between 4.1 and 4.8 depending on sample preparation and our calculated coordination numbers are all within this range. In general, the amorphous models have a low percentage of Al_{VI}, which is in agreement with the experiments and other theoretical studies. The observed trend is that the percentage of Al_{VI} and Al_V becomes larger while the percentage of Al_{IV} becomes smaller as the density increases. We find a small percentage of Al_{III} for densities 2.9 and 3.1 g/cm^3, that is absent for 3.3 g/cm^3, which agrees with the MD simulations. Overall MD studies, experiments, and our results agree in that the majority of the aluminum ions are found in Al_{IV} and Al_V environments in the amorphous phase.

In Fig. 1 we show the total neutron and partial distribution functions for a-Al_2O_3 at $\rho = 3.3$ g/cm^3. The curves for the other densities studied here have not been included in Fig. 1 since they are similar in shape to the curve for $\rho = 3.3$ g/cm^3. The graph at the top in Fig. 1 is the calculated total neutron weighted pair distribution function $g_N(r)$,[25]

$$g_N(r) = \frac{\sum_{\alpha\beta} c_\alpha b_\alpha c_\beta b_\beta g_{\alpha\beta}(r)}{\left(\sum_\alpha c_\alpha b_\alpha\right)^2}, \tag{8}$$

where $g_{\alpha\beta}$ is the partial pair distribution function, $c_{\alpha,\beta}$ is the concentration for species α and β, respectively, and $b_{\alpha,\beta}$ denotes the coherent neutron scattering length of species α and

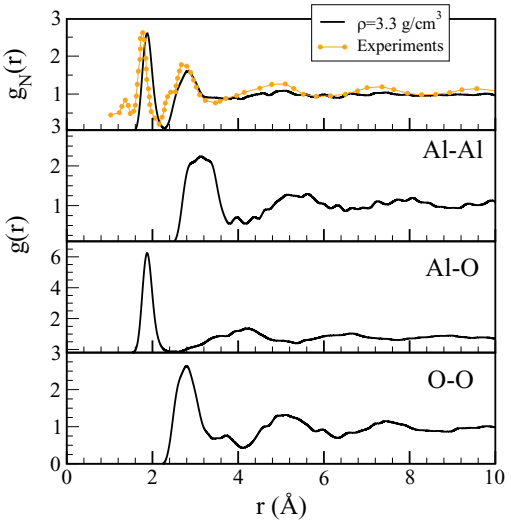

FIG. 1. (Color online) Total neutron and partial radial distribution functions for a-Al_2O_3 for a representative density, 3.3 g/cm^3. Experimental values (solid circles) were obtained from Ref. 14 and the thin line is intended as guide for the eye.

β, respectively. The values employed here are $b_{Al} = 0.3449 \times 10^4$ Å and $b_O = 0.5805 \times 10^4$ Å.[25] The experimental results from Ref. 14, obtained by an XRD study are also displayed in the graph for comparison. The positions of the first and second peaks in g_N are, respectively, 1.86 and 2.91 Å for $\rho = 2.9$ g/cm^3, 1.86 and 2.8 Å for $\rho = 3.1$ g/cm^3, and 1.86 and 2.77 Å for $\rho = 3.3$ g/cm^3. These numbers compare very well with both the MD (1.76 and 2.79 Å) and the experimental (1.8 and 2.8 Å) results.

A small shoulder can be observed around 2.4 Å in the second peak of the experimental g_N from Ref. 14 that is not present in our theoretical RDF. The feature is also not described by MD simulations.[25,26] The authors in Ref. 25 speculate that one possible explanation is that many-body effects are unaccounted for in the parametrization of their pair potential. The fact that our first-principles method agrees with the MD results indicates another origin of this feature. Instead, the feature may be a trace of intermixed crystalline phases in the experiment or due to correlation effects that the GGA implementation in our method fails to describe correctly. There is also a small peak at ∼1.6 Å in the experimental g_N that the authors of the experimental study associates to S-O correlations due to the presence of a small percentage of sulfur in the sample.

The calculated partial distribution functions are shown in the last three panels of Fig. 1. The distance to the minimum after the first peak, $R_{\alpha\beta}$, in partial distribution functions is generally taken as a cutoff used in the integration of the first peak of the RDFs to determine coordination numbers. We obtain $R_{\text{Al-Al}} = 3.85$, 3.94, and 3.78 Å for $\rho = 2.9$, 3.1, and 3.3 g/cm^3, respectively. For $R_{\text{Al-O}}$ we find 2.3, 2.31, 2.33 Å and finally for $R_{\text{O-O}}$ we obtain 3.54, 3.54, and 3.4 Å. These numbers are in accord with the MD simulations. There is a small peak around ∼1.6 Å in the partial distribution function O-O, for both $\rho = 2.9$ and 3.1 g/cm^3 (data not shown). However, the contribution of this peak is too small to be observed in the total calculated RDF. A close inspection of the supercells revealed one O atom located at 1.56 Å from another O atom at those densities. Although it is a weak signal, this suggests yet another interpretation of the 1.6 Å peak in the measured RDF as O-O pairs that are trapped in the amorphous matrix. Finally, we point out that the reason why our calculated RDFs appear to be jagged, especially around and after the second peak, is due to the relatively poor statistics of our unit cells.

Another very useful tool to investigate local structures in amorphous materials is the ADFs. Figure 2 displays the ADFs for densities 2.9, 3.1, and 3.3 g/cm^3. In order to calculate the ADFs we used the cutoffs for $R_{\text{Al-Al}}$, $R_{\text{Al-O}}$, and $R_{\text{O-O}}$ obtained from our RDFs for each density, respectively. From Table II we conclude that a-Al_2O_3 is composed mainly of Al four-coordinated and Al five-coordinated units. In an ideal tetrahedron the O-Al-O bond angle is 109.47°, the O-O-O bond angle is 60°, and the Al-O-O bond angle is 35.26°. In Fig. 2 in the lowest left corner graph, O-Al-O angles are shown and we observe a broad peak around 90°. For the lowest density the peak is located at 104.12° and it has a shoulder around 85.6°. At the intermediate density the peak is at 85.57° with a shoulder at 102.43° and at the highest density the peak is split in two, 83.04° and 94.84°. The lowest right corner graph shows O-O-O bond angles that have a peak at 59.85° for all densities.

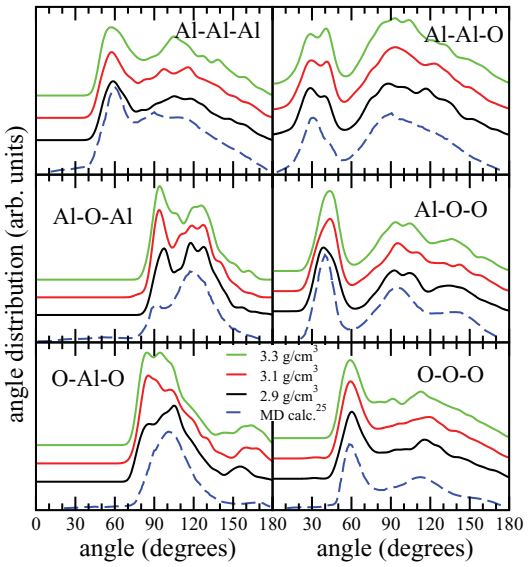

FIG. 2. (Color online) The ADFs for a-Al_2O_3 at three different densities: 2.9, 3.1, and 3.3 g/cm^3. For comparison the results of an MD run from Ref. 25 are also included (dashed line).

The graph for Al-O-O has a main peak at 37.93°, 42.99°, and 41.31° for 2.9, 3.1, and 3.3 g/cm^3, respectively. These results are in agreement with a previous MD simulation[25] and show the distortion of our fourfold units compared to the ideal tetrahedron. The main difference between our results and the MD simulation appears in the Al-O-Al bond angle plot for the highest two densities. In this graph we see two peaks. The first peak is at 97.6°, 93.2°, and 93.7° for the three respective densities. The second peak located around 120° is wider and is composed of several peaks. The MD study finds the main peak at 120° and a small shoulder of the peak at 90°.

All these statistical measurements, that is, RDFs, ADFs, coordination numbers, and nearest-neighbors bond length demonstrate that our models of a-Al_2O_3 indeed describe the amorphous state of alumina well when compared to experimental data[13–15] and other theoretical studies.[25]

B. Calculated XPS spectra

From top to bottom Fig. 3 shows, in order of decreasing density, the calculated Al $2p$ XPS spectra of α, κ, bixbyite, θ, γ, and amorphous alumina at 3.3, 3.1, and 2.9 g/cm^3. The energy reference has been taken to be α-Al_2O_3. The bars in Fig. 3 indicate local atomic energy shifts and the height of the bars denotes number of oxygen neighbors in the local environment.

The spectrum for α-alumina consists of a single peak corresponding to Al_{VI} local environments. For κ-alumina, we observe one broad peak with contributions from Al_{VI} and Al_{IV} that overlap greatly. As expected, due to its highly ordered structure, the bixbyite spectrum shows one sharp peak with contributions from only Al_{VI}. The spectrum of θ-alumina has two peaks (Al_{IV} and Al_{VI}) separated by a very small binding energy difference of 0.4 eV. The peaks are identical, which shows that the two environments, Al_{IV} and Al_{VI}, are present in the same percentage. It is worth mentioning here that depending on the simulated resolution we use when we sum the site-dependent binding-energy differences, these two peaks

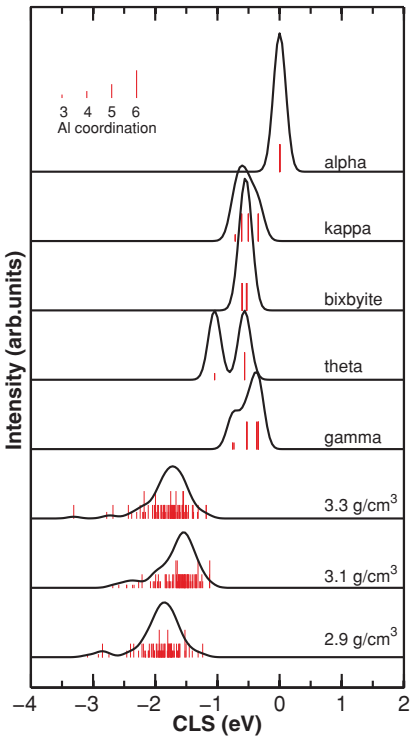

FIG. 3. (Color online) The calculated Al $2p$ XPS spectra for (from top to bottom) α, κ, bixbyite, θ, γ, and amorphous alumina at three different densities, 3.3, 3.1, and 2.9 g/cm^3. The core level shifts are shown with respect to α-alumina. The bars indicate Al energy shifts and the height of the bars denotes number of oxygen neighbors.

may merge into one or remain separated.[49] The spectrum for γ-alumina consists of one peak with a small shoulder, showing that γ-Al_2O_3 has Al ions in sixfold and fourfold coordination but their binding energy difference is too small to be well resolved. It can be seen in the amorphous spectra that a single broad Al $2p$ peak is built up by contributions from Al_{IV}, Al_V, and Al_{VI} and for the two lowest densities also by Al_{III}. All these contributions are overlapping to the extent that they cannot be resolved even with infinite resolution. We do, however, see a tendency of the low coordinated Al ions to contribute in the left tail of the main peak.

A trend observed in all calculated XPS spectra is that as the density becomes lower, the Al $2p$ peak moves toward smaller binding energies. We speculate that this shift is a consequence of a somewhat more efficient screening of the core hole due to Urbach tails that makes the band gap narrower for the more disordered structures, thereby increasing the electron mobility.

Snijders *et al.*[19] measured the XPS spectra for ultrathin Al oxide films, as grown by dry, thermal oxidation for various oxidation times within the temperature range of 373 K–773 K. They measured the binding energies throughout the transition between the amorphous state and γ-alumina, finding the energy difference between the peaks for γ-alumina and the amorphous phase to be 0.97 eV. This value is in excellent agreement with our theoretical value of 1.2 to 1.0 eV depending on the amorphous density.

Other XPS measurements[18] have obtained spectra for α, θ, η, γ, and amorphous alumina. Their measured spectra consist of a single, almost symmetrical peak for each phase. The position of this peak moves toward higher values of the binding energy as the density of the phases becomes lower. They found an energy difference of 0.61 eV between the peaks of α- and a-Al_2O_3. The authors in Ref. 18 reported broad peaks and difficulties on the curve-fitting procedure of the XPS spectra because of wide overlapping of Al_{IV} and Al_{VI} signals. Moreover, the fact that their peak moves toward higher binding energies as the density of the alumina film decreases may be attributed to charging shifts of the reference carbon 1s peak that was used in the experiment.

We speculate that the fact that XPS does not clearly distinguish between the different chemical environments of the Al^{3+} ions may be understood as a consequence of the strong ionicity of alumina. As the x-ray photon excites the Al $2p$ state it produces a core hole in the sample and the charge rearranges in order to screen the hole. In the case of Al^{3+} ions in alumina, the charge transfer to oxygen is nearly complete in all polymorphs as well as in the amorphous phase so that the on-site screening changes very little between the different polymorphs as well as between local atomic environments in the amorphous structure.

C. NMR simulations

In Fig. 4 we present the calculated ^{27}Al NMR spectra for (from top to bottom) α, κ, bixbyite, θ, γ, and amorphous alumina at three different densities, 3.3, 3.1, and 2.9 g/cm^3. The bars in the figure correspond to site-dependent NMR

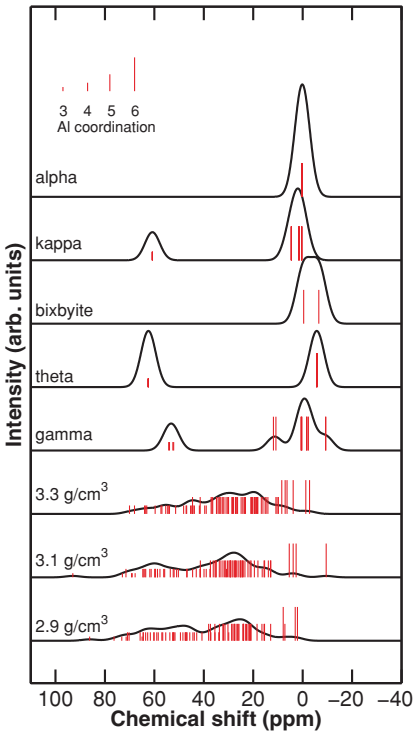

FIG. 4. (Color online) The calculated ^{27}Al NMR spectra for (from top to bottom) α, κ, bixbyite, θ, γ, and amorphous alumina at three different densities, 3.3, 3.1, and 2.9 g/cm^3. The bars indicate site-dependent NMR chemical shifts and the height of the bars indicates the number of oxygen neighbors of an Al site. The values of the shifts are given with respect to the theoretical α-Al_2O_3 chemical shift.

chemical shifts and the height of the bars indicates the number of oxygen neighbors of an Al site. The spectra were constructed in a similar manner as the XPS spectra. The standard deviation of the Gaussians used here is 3 ppm and the NMR chemical shifts are given with respect to the calculated shift of $\alpha =$ 532.27 ppm.

The spectrum for α-alumina consists of one peak that is built up only by contributions of Al_{VI}. There are two clear peaks in the κ-Al_2O_3 spectrum. The small peak at ~61 ppm contains the contributions from Al_{IV}, whereas the peak to the right is built up by Al_{VI}. The next spectrum corresponds to the bixbyite structure and it contains one broad peak located at −5 ppm that is built up by the contributions of two inequivalent Al_{VI} sites. There are two well-defined peaks of identical height in the spectrum of θ-Al_2O_3. The peaks are separated by ~68 ppm. The peak to the left at ~62 ppm has contributions from Al_{IV} and the peak to the right at about −6 ppm contains the contributions from Al_{VI}. These two peaks agree with the fact that θ-alumina has 50% of Al atoms in tetrahedral geometries and the other 50% are in octahedral environments.[41] The spectrum for γ-Al_2O_3 shows more complexity. It is mainly composed by two peaks. The peak to the left at ~50 ppm is the smallest and contains contributions from Al_{IV}, whereas the peak to the right at ~3 ppm is broader and has two shoulders at 13 and −8 ppm, respectively. Despite its richer structure, the latter peak is built up only by Al_{VI}. NMR experiments on γ-Al_2O_3 produce very different results, as can be seen in Table III. Indeed, the experiment that compares best with our calculation is Ref. 78, where three peaks located at 48, 19.6, and −7.9 ppm were found. In that reference the middle peak was associated to Al_V; however, the good agreement with our calculated intermediate Al_{VI} peak suggests that the 19.6 ppm peak may actually be due to six-coordinated Al as well. Other authors have supplied another explanation for the presence of the middle peak as due to the intermix of the amorphous phase in the sample.[76]

The last three spectra at the bottom of Fig. 4 correspond to a-Al_2O_3 at different densities. The small peak at around 0 ppm is composed by chemical shifts from six-coordinated Al ions. This peak has a small intensity and has a width induced by structural disorder of about 10 ppm. At around 30 ppm, we can clearly observe another peak built up mainly by fivefold-coordinated Al ions. The peak has a width induced by structural disorder of about 30 ppm. A third peak feature can be distinguished at around 60 ppm composed of contributions from fourfold-coordinated Al ions. This peak has a width induced by structural disorder of about 35 ppm. For the two lowest densities of a-Al_2O_3 there is also a small peak at ~80 ppm associated with threefold-coordinated Al. The disorder broadening of this peak is about 20 ppm. The positions of our calculated peaks and the clear resolution of local Al coordination agrees very well with measured NMR spectra.[15–17]

Table III lists the experimental and theoretical ^{27}Al NMR isotropic chemical shifts, quadrupole coupling constants,

TABLE III. Experimental and theoretical ^{27}Al NMR isotropic chemical shifts, quadrupole coupling constants and asymmetry parameters for α, κ, bixbyite, θ, γ, and amorphous alumina. Theoretical values of δ_{iso} are listed with respect to the theoretical isotropic chemical shield for α-alumina, 532.27 ppm. The experimental values of δ_{iso} are given relative to the α-alumina shift, 13.5 ppm, measured in Ref. 7. Dashes are used to indicate that data has not been measured in the experiment of the given reference. In cases where more than one reference is presented, the dashes are placed in the order of appearance of the references.

		δ_{iso} (ppm)		C_Q (MHz)		η	
Phase	Al site	Expt.	Theory	Expt.	Theory	Expt.	Theory
α-Al_2O_3[7]	Al_{VI}	0	0	2.38	2.33	0	0
	Al_{VI}	−0.5	0.26	0.5	−9.98	–	0.33
	Al_{VI}	4.5	1.36	0.85	5.2	–	0.94
κ-Al_2O_3[71]	Al_{VI}	–	4.39	–	4.51	–	0.77
	Al_{IV}	68	60.65	0.76	−5.53	0.3	0.33
	Al_{V+I}	–	–	>1.5	–	–	–
	Al_{VI}	–	−6.7	–	4.25	–	0.01
Bixbyite	Al_{VI}	–	0.55	–	8.65	–	0.45
	Al_{VI}	−3.0	−5.86	3.5	3.44	0	0.18
θ-Al_2O_3[7]	Al_{IV}	66.6	62.26	6.4	6.34	0.65	0.42
	Al_{VI}	–, –, –2	−8	–, –, 3.5	14.4	–	0
	Al_{VI}	−6.3, −6.7, 29.5	3	–, –, 5.1	−4.6	–	0.7
γ-Al_2O_3[69,76,77]	Al_{VI}	–, –, 44.5	13	–, –, 4.9	−8.8	–	0.46
	Al_{IV}	51.9, 50.7, 59	52	–, –, 5.1	5.6	–	0.3
	Al_{VI}	−7.9	–	–	–	–	–
γ-Al_2O_3[78]	Al_V	19.6	–	–	–	–	–
	Al_{IV}	48	–	–	–	–	–
	Al_{VI}	−3.5, −2, −9	0 (±5)	–	–	–	–
	Al_V	16.5, 24.5, 16.5	30 (±15)	–	–	–	–
a-Al_2O_3[15–17]	Al_{IV}	46.5, 58, 46.5	60 (±17.5)	–	–	–	–
	Al_{III}	–	80 (±10)	–	–	–	–

and asymmetry parameters for α-, κ-, bixbyite, θ-, and γ-alumina as well as our amorphous results. Here, as in Fig. 4, the theoretical isotropic chemical shield for α-alumina, 532.27 ppm, was used as a reference to calculate the theoretical values of δ_{iso}. In order to compare the calculated results and experiments on an absolute scale, we have shifted all experimental values of δ_{iso} relative to the shift of α-alumina of 13.5 ppm.[7] The values obtained for the isotropic shifts are generally in very good agreement with the experimental data, especially the peak associated to Al_{IV} coordination. Typically, this peak can be measured with a better resolution than the peak for Al ions in octahedral environments. The reason is that the peak related to Al_{VI} may broaden depending on the purity of the sample; for instance the presence of α-alumina. The situation for κ- and γ-alumina is more complicated since these phases are not well characterized. To our knowledge the experiments in Ref. 71 are the only NMR data available for κ-alumina. The authors of that study found one peak associated to Al_{IV}, two peaks corresponding to Al_{VI} coordination, and a third peak assigned to Al_{V+I}, a very distorted octahedral environment for one of the atoms which is believed to be responsible for a very broad NMR signal. However, they do not report the position of this third peak nor the values of C_Q or η. Their values of C_Q for the other peaks are an order of magnitude smaller than ours. The available data of C_Q and η is scarce in the literature for γ-alumina. The values given by Coster *et al.* in Ref. 77 are not in good agreement with the ones calculated here. We have not found any report in the literature of data for C_Q or η for the amorphous phase to compare with our values. However, we believe that the reasonably good agreement in the polymorphs supports our results on the amorphous phase.

V. CONCLUSIONS

We have presented here first-principles calculations of XPS spectra and NMR chemical shifts on a-Al_2O_3 and α, κ, bixbyite, θ, and γ. The amorphous structures were obtained by a simple and very efficient stochastic quenching method. The coordination numbers, bond length, radial distribution functions, and ADFs were calculated for a-Al_2O_3 and were found to be in excellent agreement with experiments and previous MD simulations. Thus, showing the validity of using the stochastic quenching method to find amorphous structures. Our calculated XPS spectra and NMR chemical shifts reproduce experiments well and we conclude that the problems of resolving local coordination in XPS is due to the strong ionicity of all the alumina polymorphs as well as in the amorphous structure. The coordination environments are well resolved in the calculated NMR chemical shifts, in good agreement with experiments. We have calculated the broadening of NMR peaks in the amorphous spectra due to local environment effects and found that it can be up to 35 ppm. We show that an analysis of the details of NMR spectra of amorphous alumina must consider differences in local environment for atoms with the same coordination number and Al-O distance in order to interpret the spectra correctly. Our results show that first-principles calculations can be used to interpret NMR and XPS experiments of complex structures with high accuracy.

ACKNOWLEDGMENTS

E.H. and R.L. acknowledge support from FONDECYT Projects No. 11080259 and No. 1110602 as well as DID (UACH) Grants No. SR-2008-0 and No. S-2008-51. We gratefully acknowledge the receipt of the computer resources provided by MOTT2 (EPSRC Grant No. GR/S84415/01) and HECToR (Grant No. EP/F067496/1). All structural optimizations were performed on the supercomputer Ainil at the Institute of Physics of Universidad Austral de Chile. We thank Nicolas Bock for valuable discussions and ICSD for access to the material database. C. A. acknowledges financial support from FAPITEC/CNPq.

[1] X. Nie, E. I. Meletis, J. C. Jiang, A. Leyland, A. L. Yerokhin, and A. Matthews, Surf. Coat. Technol. **149**, 245 (2002).
[2] H. Tops, B. S. Clausen, and F. E. Massoth, *Hydrotreating Catalysis—Science and Technology* (Springer-Verlag, Berlin/Heidelberg, 1996), Vol. 11.
[3] R. Prins, *Handbook of Heterogeneous Catalysis* (Wiley-VHC Verlagsgesellschaft, Weinheim, 1997), Vol. 4.
[4] R. Collongues, D. Gourier, A. Kahn, J. P. Boilot, P. Colomban, and A. Wicker, J. Phys. Chem. Solids **45**, 981 (1984).
[5] R. E. Newnham and Y. M. de Haan, Z. Kristallogr. Kristallgeom. Kristallphys. Kristallchem. **117**, 235 (1962).
[6] A. S. Barker, Phys. Rev. **132**, 1474 (1963).
[7] L. A. O'Dell, S. L. P. Savin, A. V. Chadwick, and M. E. Smith, Solid State Nucl. Magn. Reson. **31**, 169 (2007).
[8] A. I. Kingon, J. P. Maria, and S. K. Streiffer, Nature (London) **406**, 1032 (2000).
[9] P. Yang, D. Zhao, D. I. Margolese, B. F. Chmelka, and G. D. Stucky, Nature (London) **396**, 152 (1998).
[10] M. J. de Castro, R. Serna, J. A. Chaos, C. N. Afonso, and E. R. Hodgson, Nucl. Instrum. Methods B **166–167**, 793 (2000).
[11] J. L. Deschanvres, W. Meffre, J. C. Joubert, J. P. Senateur, F. Robaut, J. E. Broquin, and R. Rimet, J. Alloys Compd. **275–277**, 742 (1998).
[12] V. B. Lazarev, G. P. Panasyuk, I. L. Voroshilov, Boudova, M. N. Danchevskaya, S. N. Torbin, and Y. D. Ivakin, Ind. Eng. Res. **35**, 3721 (1996).
[13] Y. Oka, T. Takahashi, K. Okada, and S. I. Iwai, J. Non-Cryst. Solids **30**, 349 (1979).
[14] P. Lamparter and R. Kniep, Physica B **234–236**, 405 (1997).
[15] S. K. Lee, S. B. Lee, S. Y. Park, Y. S. Yi, and C. W. Ahn, Phys. Rev. Lett. **103**, 095501 (2009).
[16] I. Farnan, R. Dupree, Y. Jeong, G. E. Thompson, G. C. Wood, A. J. Forty, J. P. Senateur, F. Robaut, J. E. Broquin, and R. Rimet, Thin Solid Films **173**, 209 (1999).
[17] G. Kunath-Fandrei, T. J. Bastow, J. S. Hall, C. Jäger, and M. E. Smith, J. Phys. Chem. **99**, 15138 (1995).
[18] Y. Kameshima, A. Yasumori, and K. Okada, J. Surf. Sci. Soc. Jpn. **21**, 481 (2000).

[19]P. C. Snijders, L. P. H. Jeurgens, and W. G. Sloof, Surf. Sci. **589**, 98 (2005).
[20]C. S. Bhatia, G. Guthmiller, and A. M. Spool, J. Vac. Sci. Technol. A **7**, 1298 (1989).
[21]K. Koski, J. Hölsä, and P. Juliett, Thin Solid Films **339**, 240 (1999).
[22]H. Momida, T. Hamada, Y. Takagi, T. Yamamoto, T. Uda, and T. Ohno, Phys. Rev. B **73**, 054108 (2006).
[23]P. H. Poole, T. Grande, F. Sciortino, H. E. Stanley, and C. Austen Angel, Comput. Mater. Sci. **4**, 373 (1995).
[24]S. Aasland and P. F. McMillan, Nature (London) **369**, 633 (1994).
[25]G. Gutiérrez and B. Johansson, Phys. Rev. B **65**, 104202 (2002).
[26]V. van Hoang and S. K. Oh, Physica B **352**, 73 (2004).
[27]P. Hohenberg and W. Kohn, Phys. Rev. B **136**, 864 (1964).
[28]W. Kohn and L. J. Sham, Phys. Rev. **140**, A1133 (1965).
[29]C. Arrouvel, D. Costa, B. Diawara, and P. Marcus, J. Phys. Chem. C **111**, 18164 (2007).
[30]C. Arrouvel, M. Breysse, H. Toulhoat, and P. Raybaud, J. Catal. **226**, 260 (2004).
[31]A. Amézaga, E. Holmström, R. Lizárraga, E. Menendez-Proupin, P. Bartolo-Perez, and P. Giannozzi, Phys. Rev. B **81**, 014210 (2010).
[32]R. Lizárraga, E. Holmström, A. Amézaga, N. Bock, T. Peery, E. Menendez-Proupin, and P. Giannozzi, J. Mater. Sci. **18**, 5071 (2010).
[33]S. E. Ashbrook, M. Cutajar, C. J. Pickard, R. I. Walton, and S. Wimperis, Phys. Chem. Chem. Phys. **10**, 5754 (2008).
[34]E. Holmström, N. Bock, T. B. Peery, R. Lizárraga, G. De Lorenzi-Venneri, E. D. Chisolm, and D. C. Wallace, Phys. Rev. E **80**, 51111 (2009).
[35]E. Holmström, N. Bock, T. Peery, E. Chisolm, R. Lizárraga, G. De Lorenzi-Venneri, and D. Wallace, Phys. Rev. B **82**, 024203 (2010).
[36]N. Bock, E. Holmström, T. B. Peery, R. Lizárraga, E. D. Chisolm, G. De Lorenzi-Venneri, and D. C. Wallace, Phys. Rev. B **82**, 144101 (2010).
[37]G. Kresse and J. Hafner, Phys. Rev. B **49**, 14251 (1994).
[38]J. Hafner [http://cms.mpi.univie.ac.at/vasp/].
[39]R. W. G. Wyckoff, *Crystal Structures* (Wiley, New York, 1964).
[40]L. Smrcok, V. Langer, M. Halvarsson, and S. Ruppi, Z. Kristallogr. **216**, 409 (2001).
[41]E. Husson and Y. Repelin, Eur. J. Solid State Inorg. Chem. **33**, 1223 (1996).
[42]X. Krokidis, P. Raybaud, A.-E. Gobichon, B. Rebours, P. Euzen, and H. Toulhoat, J. Phys. Chem. B **105**, 5121 (2001).
[43]W. Olovsson, E. Holmström, J. Wills, P. James, I. A. Abrikosov, and A. M. N. Niklasson, Phys. Rev. B **72**, 155419 (2005).
[44]W. Olovsson, E. Holmstrom, A. Sandell, and I. A. Abrikosov, Phys. Rev. B **68**, 045411 (2003).
[45]E. Holmström, W. Olovsson, I. Abrikosov, A. Niklasson, B. Johansson, M. Gorgoi, O. Karis, S. Svensson, F. Schäfers, W. Braun, G. Öhrwall, G. Andersson, M. Marcellini, and W. Eberhardt, Phys. Rev. Lett. **97**, 266106 (2006).
[46]B. Johansson and N. Maartensson, Phys. Rev. B **21**, 4427 (1980).
[47]W. Olovsson, C. Göransson, L. V. Pourovskii, B. Johansson, and I. A. Abrikosov, Phys. Rev. B **72**, 064203 (2005).
[48]J. F. Janak, Phys. Rev. B **18**, 7165 (1978).
[49]We choose the value of 0.1 eV as the standard deviation of the Gaussians to obtain the XPS spectra in order to simulate the resolution of an XPS apparatus.
[50]F. Mauri, B. G. Pfrommer, and S. G. Louie, Phys. Rev. Lett. **77**, 5300 (1996).
[51]C. J. Pickard and F. Mauri, Phys. Rev. B **63**, 245101 (2001).
[52]J. R. Yates, T. N. Pham, C. J. Pickard, F. Mauri, A. M. Amado, A. M. Gil, and S. P. Brown, J. Am. Chem. Soc. **127**, 10216 (2005).
[53]M. Profeta, F. Mauri, and C. J. Pickard, J. Am. Chem. Soc. **125**, 541 (2003).
[54]P. Pyykkö, Mol. Phys. **106**, 1965 (2008).
[55]J. P. Perdew, K. Burke, and M. Ernzerhof, Phys. Rev. Lett. **77**, 3865 (1996).
[56]P. E. Blöchl, Phys. Rev. B **50**, 17953 (1994).
[57]H. J. Monkhorst and J. D. Pack, Phys. Rev. B **13**, 5188 (1976).
[58]M. D. Segall, P. J. D. Lindan, M. J. Probert, C. J. Pickard, P. Hasnip, S. J. J. Clark, and M. C. Payne, J. Phys.: Condens. Matter **14**, 2717 (2002).
[59]S. Geller, Acta Crystallogr., Sect. B: Struct. Crystallogr. Cryst. Chem. **B 27**, 821 (1971).
[60]L. Smrcok, V. Langer, and J. Krestan, Acta Crystallogr., Sect. C **62**, I83 (2006).
[61]C. Pecharroman, I. Sobrados, and J. E. Iglesias, J. Phys. Chem. B **103**, 6160 (1999).
[62]G. Gutiérrez, A. Taga, and B. Johansson, Phys. Rev. B **65**, 012101 (2001).
[63]G. Paglia, A. L. Rohl, C. E. Buckley, and J. D. Gale, Phys. Rev. B **71**, 224115 (2005).
[64]I. Levin and D. Brandon, J. Am. Ceram. Soc. **81**, 1995 (1998).
[65]M. Digne, P. Sautet, P. Raybaud, P. Euzen, and H. Toulhoat, J. Catal. **226**, 54 (2004).
[66]M. Digne, P. Raybaud, P. Sautet, B. Rebours, and H. Toulhoat, J. Phys. Chem. B **110**, 20719 (2006).
[67]C. Arrouvel, M. Digne, M. Breysse, H. Toulhoat, and P. Raybaud, J. Catal. **222**, 152 (2004).
[68]M. Digne, P. Sautet, P. Raybaud, P. Euzen, and H. Toulhoat, J. Catal. **211**, 1 (2002).
[69]M. H. Lee, C. F. Cheng, V. Heine, and J. Klinowski, Chem. Phys. Lett. **265**, 673 (1997).
[70]R. S. Zhou and R. L. Snyder, Acta Crystallogr., Sect. B: Struct. Sci. **47**, 617 (1991).
[71]B. Ollivier, R. Retoux, P. Lacorre, D. Massiot, and G. Ferey, J. Mater. Chem. **7**, 1049 (1997).
[72]T. Yokokawa and O. J. Kleppa, J. Phys. Chem. **68**, 3246 (1964).
[73]C. Ruberto, Y. Yourdshahyan, and B. I. Lundqvist, Phys. Rev. B **67**, 195412 (2003).
[74]C. Wolverton and K. C. Hass, Phys. Rev. B **63**, 024102 (2000).
[75]The XRD experiments performed by Oka et al. (Ref. 13) obtained two values of the coordination number for Al corresponding to two samples prepared in sulfuric acid using ac and dc polarizing voltages, respectively.
[76]G. Paglia, C. E. Buckley, A. L. Rohl, B. A. Hunter, R. D. Hart, J. V. Hanna, and L. T. Byrne, Phys. Rev. B **68**, 144110 (2003).
[77]D. Coster, A. L. Biumenfeld, and J. J. Fripiat, J. Phys. Chem. **98**, 6201 (1994).
[78]J. A. Wang, X. Bokhimi, A. Morales, O. Novaro, T. López, and R. Gómez, J. Phys. Chem. B **103**, 299 (1999).